NOVEL APPROACH TO ANALYTICAL MODELLING OF STEADY-STATE HEAT TRANSFER FROM THE EXTERIOR OF TEFC INDUCTION MOTORS

by

Dardan O. KLIMENTA[a,b*] and Antti HANNUKAINEN[a]

[a] Department of Mathematics and Systems Analysis, Aalto University, Aalto, Finland
[b] Faculty of Technical Sciences, University of Pristina in Kosovska Mitrovica, Kosovska Mitrovica, Serbia

Original scientific paper
https://doi.org/10.2298/TSCI150629091K

The purpose of this paper is to propose a novel approach to analytical modelling of steady-state heat transfer from the exterior of totally enclosed fan-cooled induction motors. The proposed approach is based on the geometry simplification methods, energy balance equation, modified correlations for forced convection, the Stefan-Boltzmann law, air-flow velocity profiles, and turbulence factor models. To apply modified correlations for forced convection, the motor exterior is presented with surfaces of elementary 3-D shapes as well as the air-flow velocity profiles and turbulence factor models are introduced. The existing correlations for forced convection from a short horizontal cylinder and correlations for heat transfer from straight fins (as well as inter-fin surfaces) in axial air-flows are modified by introducing the Prandtl number to the appropriate power. The correlations for forced convection from straight fins and inter-fin surfaces are derived from the existing ones for combined heat transfer (due to forced convection and radiation) by using the forced-convection correlations for a single flat plate. Employing the proposed analytical approach, satisfactory agreement is obtained with experimental data from other studies.

Key words: *analytical model, empirical correlation, energy balance, steady-state heat transfer, totally enclosed fan-cooled induction motor*

Introduction

Existing analytical models of steady-state heat transfer in totally enclosed fan-cooled (TEFC) induction motors are based on a number of commonly accepted assumptions [1-8] and application of the lumped-parameter circuits. However, as the authors will demonstrate, some of these assumptions are unrealistic. In addition, as a rule, analytical modelling of steady-state heat transfer in a solid should begin by setting up only one energy balance equation for its entire outer surface. This was not the case with TEFC induction motors from the first analytical models up to the present day. Therefore, lumped-parameter models may not be accurate enough and adequate for precise modelling of heat transfer processes in electrical machines. In order to accurately model steady-state heat transfer from the motor exterior it is necessary to avoid unrealistic assumptions and lumped-parameters. In the present paper, this is achieved by using the geometry simplification methods, energy balance equation, empirical correlations

* Corresponding author, e-mail: dardan.klimenta@aalto.fi; dardan.klimenta@pr.ac.rs

(including the Stefan-Boltzmann law), air-flow velocity profiles from [9], and turbulence factor models from [9].

Some of the unrealistic assumptions commonly used in thermal modelling of TEFC induction motors are: (1) that the heat transfer coefficient due to forced convection can only depend on the turbulence factor, $K_{\xi,y}$, and/or the air-flow velocity at the beginning of the cooling channels, V_0 [1-3], (2) that the correlations which were experimentally determined for a combination of forced convection and radiation from [4, 5] can directly be applied to the modelling of only the forced convection as in [3], (3) that the air-flow velocity at the beginning of the cooling channels, V_0, always amounts to approximately 70% or 75% of the peripheral velocity of the fan wheel, V_p, [2, 3], (4) that the cooling fins should only increase the heat transfer between the motor exterior and the surroundings [6, 7], which is not consistent with the results presented in [4, 5], (5) that the end-windings do not dissipate heat to the air inside the end-winding zones of the motor, and the heat generated by the stator winding is completely transferred to the stator core [8], *etc.* In quite a large number of existing analytical models, to a greater or lesser extent, these or similar assumptions adversely affect the model accuracy.

More accurate analytical thermal model should be developed by using: (1) the motor geometry simplification that does not involve changes in the outer surface areas of the frame and end-shields, as well as the motor radius under the cooling fins, (2) the selection of empirical correlations for forced convection appropriate to the particular flow conditions and shapes within the equivalent geometric representation of the motor exterior, (3) a *good* polynomial approximation to estimate profiles of air-flow velocity, V_y, along the frame cooling channels [9], and (4) an appropriate model to estimate reduction of the turbulence factor, $K_{\xi,y}$,along the frame cooling channels [9].

The thermal model proposed in this paper is based on a simplified geometric representation of the exterior of TEFC induction motors under different load conditions by using surfaces of elementary 3-D shapes. The model proposed in this paper considers an equivalent combination/representation of surfaces of 3-D geometric shapes to simplify the exterior of TEFC induction motors operating under different loads. All the surfaces have their own heat transfer coefficients due to forced convection and radiation. The coefficients represent unknowns in the energy balance equation and their values have been estimated with the appropriate empirical correlations. Moreover, the suggested approach to thermal modelling has been applied to two TEFC induction motors having different pole numbers, shaft heights, and rated powers; both operating in two different regimes.

Equivalent geometric representation of the motor exterior

From an empirical point of view, pulley, metal nameplate, eyebolt, metal keys of the shaft, fan wheel and cowl do not have a significant effect on the heat transfer between the motor exterior and the surroundings. Hence, these elements additionally complicate the equivalent geometric representation of the motor shape. For this reason, the elements are not included into the present geometric model.

Forced convection and radiation from the shaft extensions are disabled by the pulley and the fan wheel. Therefore, the surfaces of the shaft extensions are assumed to be cylindrical and adiabatic. Motor elements such as terminal box and mounting feet have complex shapes and outer surface areas of considerable sizes. These two elements are difficult to model thermally and geometrically, and their effect can not be ignored. Moreover, end-shields are usually hollow (the shaft passes through the end-shields), externally-finned and not ideally flat and/or cylindrical.

Modelling the geometry of the TEFC induction motor elements (main parts and those with significant surfaces) for the purpose of their thermal analysis will be based on empirically confirmed facts. These empirical facts are: (1) if there is any change in the motor outer surface during the procedure of geometry modelling, its heat transfer coefficients need to be recalculated accordingly [10], (2) a change in the number of cooling fins up to 12 and an appropriate change in the spacing between the fins do not affect significantly their heat transfer coefficients [6, 7], (3) a small change in the height of cooling fins with regard to its optimal value will not have significant effect on the fin efficiency [11] and corresponding heat transfer coefficients [6, 7], (4) a change in the number of cooling fins will not cause any significant change in the air-flow velocity at the beginning of the cooling channels, V_0 [6, 7], (5) the one-nth-power law can be applied in a case of air-flow through the annular gap between two coaxial tubes [12-15], and (6) the degree of flow turbulence depends very little on the air-flow velocity [16].

In order to simplify the geometry of a TEFC induction motor, its shape is represented by a union of rotating and stationary horizontal cylinders with and without fins, where a number of lengths and one radius differ from the corresponding actual dimensions. In the following paragraphs and equations, radii, r_{iE}, lengths/thicknesses, L_{iE}, and surfaces, S_{iE}, labelled with a combination of surface numbers i = 1-10 and capital letter E differ from the corresponding actual dimensions of the motor. Radii, r_i, lengths/thicknesses, L_i, and surfaces, S_i, labelled only with surface numbers i = 1-10 are introduced in order to display the equations related to the steady-state heat transfer model in a more convenient manner. The surface numbers i = 1-10 (that is, subscripts) are used for the labelling as shown in fig. 1. All radii and lengths are in meters, and surface areas are in m^2.

The exterior of a TEFC induction motor, in the direction of fan wheel from the drive end of the shaft, is represented by a combination of surfaces composed of: (S_1) the base surface of a rotating disk having radius r_1, thickness L_1 = 0 m and base area S_1, (S_2) the lateral surface of a rotating horizontal cylinder having radius $r_2 = r_1$, length $L_2 = L_{2E}$ and lateral area $S_2 = S_{2E}$, (S_3) the ring-shaped base surface of a stationary horizontal hollow cylinder having outer radius r_3, length $L_3 = L_{3E}$ and base area $S_3 = S_{3E}$, (S_4) the lateral surface of a stationary horizontal cylinder having radius r_4, length $L_4 = L_{3E}$ and lateral area $S_4 = S_{4E}$, (S_5) all the fin surfaces of a stationary horizontal longitudinally-finned cylinder having radius over the fins $r_5 = r_{5E}$, length L_5 and total fin area $S_5 = S_{5E}$, (S_6) all the inter-fin surfaces of a stationary horizontal longitudinally-finned cylinder having radius under the fins $r_6 = r_3$, length $L_6 = L_5$ and total inter-fin area $S_6 = S_{6E}$, (S_7) the lateral surface of a stationary horizontal cylinder having radius $r_7 = r_3$, length $L_7 = L_{7E}$ and lateral area $S_7 = S_{7E}$, (S_8) the ring-shaped base surface of a stationary horizontal

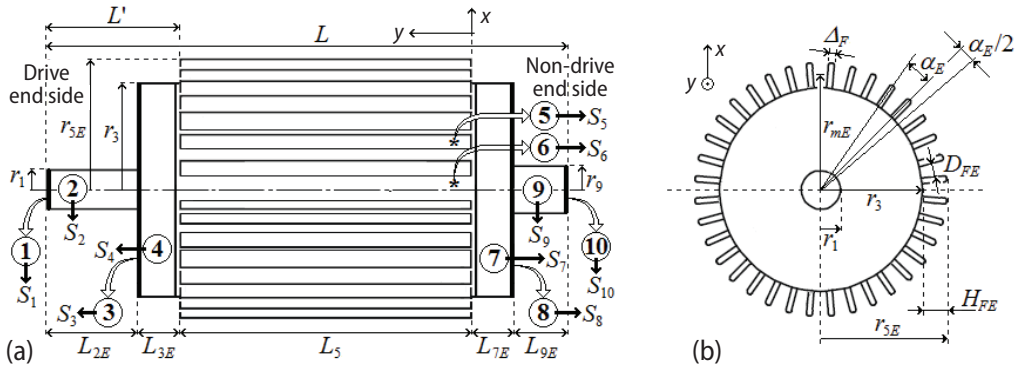

Figure 1. Equivalent TEFC induction motor; (a) side view, (b) view from the drive end side

hollow cylinder having outer radius $r_8 = r_3$, length $L_8 = L_{7E}$ and base area $S_8 = S_{8E}$, (S_9) the lateral surface of a rotating horizontal cylinder having radius r_9, length $L_9 = L_{9E}$ and lateral area $S_9 = S_{9E}$, and (S_{10}) the base surface of a rotating disk having radius $r_{10} = r_9$, thickness $L_{10} = 0$ m and base area S_{10}. Equivalent geometric representation of a TEFC induction motor by using the S_1, S_2, …, S_9 and S_{10} surfaces, that is, the equivalent TEFC induction motor is shown in fig. 1.

The equivalent dimensions are determined such that surface areas of the equivalent geometric representations of the frame and end-shields match with the actual surface areas of the same elements. According to this principle, $S_{3E} + S_{4E}$ is the actual outer surface area of the drive end-shield, $S_{7E} + S_{8E}$ is the actual outer surface area of the non-drive end-shield, and S_{3E} is equal to S_{8E}. Moreover, $S_{5E} + S_{6E}$ is the actual outer surface area of the finned frame, terminal box and two mounting feet.

Basic calculations lead to the following formulas:

$$L_{2E} = L' - L_{3E} \tag{1}$$

$$L_{3E} = \frac{S_{3E} + S_{4E} - \pi(r_3^2 - r_9^2)}{2\pi r_3} \tag{2}$$

$$L_{7E} = \frac{S_{7E} + S_{8E} - \pi(r_3^2 - r_9^2)}{2\pi r_3} \tag{3}$$

$$L_{9E} = L - L_{2E} - L_{3E} - L_5 - L_{7E} \tag{4}$$

$$r_{5E} = r_3 + H_{FE} \tag{5}$$

where L' is the distance from the flat surface of the drive shaft extension to the end of the cooling channels, L – the length of the shaft, and H_{FE} – the height of the equivalent cooling fins in m, which according to fig. 1(b) is:

$$H_{FE} = \frac{S_{5E} + S_{6E} - 2\pi r_3 L_5}{2L_5 N_{FE}} \tag{6}$$

where N_{FE} is the number of the equivalent cooling fins (an integer value). Also, according to fig. 1(b), the width of the equivalent cooling channels (that is, the spacing between equivalent fins) at half the height H_{FE} in meters is:

$$D_{FE} = 2r_{mE}\sqrt{1 - \cos^2\frac{\alpha_E}{2}} - \Delta_F \tag{7}$$

where $r_{mE} = (r_3 + r_{5E})/2$ is the radius of the circle which divides the equivalent fins into two halves, Δ_F – the thickness of an actual cooling fin, and $\alpha_E = 360/N_{FE}$ – the angle between the radial axes of every two adjacent equivalent fins in degrees. The radial axis of an equivalent fin represents a straight line passing through the center points of the shaft and the equivalent fin. Moreover, in accordance with fig. 1, x is the distance from the fin base measured along the radial axis in m.

Model for steady-state heat transfer from the motor exterior

The steady-state heat transfer from the exterior of the equivalent TEFC induction motor is discussed in this section and illustrated in fig. 2. The average values of the heat transfer coeffi-

cients are calculated using the law of conservation of energy, empirical correlations for forced convection, radiation and air-flow velocity profiles, and turbulence factor models. The parameters displayed in fig. 2 have the following meanings: V_1 [ms^{-1}] is the air-flow velocity at the end of the cooling channels (obtained by means of the appropriate air-flow velocity profile from [9]), T_s [K] – the average temperature of the outer surface of the equivalent motor, T_a [K] – the temperature of the surrounding air, and y [m] – the longiudinal distance from the fan cowl. Moreover, $Q_{c1,s}$, $Q_{c2,s}$,…, $Q_{c9,s}$, and $Q_{c10,s}$ [Wm^{-2}] are the heat fluxes due to forced convection from the S_1, S_2, …, S_9, and S_{10} surfaces to the surrounding air, respectively. The surface $S_3 = \pi(r_3^2 - r_9^2)$ represents the area of the ring-shaped surface between the two concentric circles with radii r_2 and r_9, $S_4 = 2\pi r_3 L_{3E}$ – the lateral surface area of the cylinder with outer radius r_3 and length L_{3E}, $S_5 = N_{FE}[(2H_{FE} + \Delta_F)L_5 + 2H_{FE}\Delta_F]$ – the surface area of all the equivalent cooling fins including surface areas of their tips and sides, $S_6 = (2\pi r_3 - N_{FE}\Delta_F)L_5$ – the area of all the surfaces amongst the equivalent cooling fins, $S_7 = 2\pi r_3 L_{7E}$ – the lateral surface area of the cylinder with outer radius r_3 and length L_{7E}, and $S_8 = S_3$. The fluxes $Q_{r1,s}$, $Q_{r2,s}$, …, $Q_{r9,s}$, and $Q_{r10,s}$ [Wm^{-2}] are the heat fluxes due to radiation from the S_1, S_2,…, S_9 and S_{10} surfaces to the surroundings, respectively.

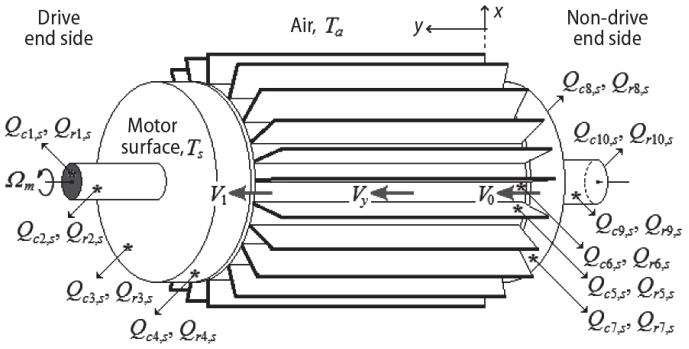

Figure 2. Heat transfer processes from the exterior of the equivalent TEFC induction motor to the surroundings

Initially the whole structure of the equivalent TEFC induction motor is assumed to be at a constant temperature, T_s, and to transfer heat from all the aforementioned surfaces except S_2 and S_9 to the surroundings by forced convection and radiation. All the surfaces except S_2 and S_9 are also assumed to be at constant, but different heat fluxes. The surfaces S_2 and S_9 are assumed to be adiabatic. Moreover, it is assumed that the heat transfer coefficients for the fin surfaces, S_5, the fin tips, $\Delta_F L_5$, and the fin sides, $\Delta_F H_{FE}$, have the same values; that the materials are homogenous and isotropic, that the shaft rotation does not affect the heat transfer due to radiation from the flat surfaces of the shaft extensions to the surroundings; that there is no longitudinal heat conduction in the frame, fins and cylindrical parts of the two end-shields; as well as that there is no radial heat conduction in the disk-shaped parts of the two end-shields.

The heat transfer coefficients corresponding to the forced-convection processes $Q_{c1,s}$, $Q_{c2,s} = 0$,…, $Q_{c9,s} = 0$, and $Q_{c10,s}$ [Wm^{-2}] are h_{c1}, $h_{c2} = 0$, …, $h_{c9} = 0$, and h_{c10} [Wm^{-2}K^{-1}], respectively. Also, the heat transfer coefficients corresponding to the radiation processes $Q_{r1,s}$, $Q_{r2,s} = 0$,…, $Q_{r9,s} = 0$, and $Q_{r10,s}$ [Wm^{-2}] are h_{r1}, $h_{r2} = 0$, …, $h_{r9} = 0$, and h_{r10} [Wm^{-2}K^{-1}], respectively. Assuming a number of the previously-mentioned parameters are mutually equal, the rates of heat transfer processes by forced convection Q_{c1}, $Q_{c2} = 0$,…, $Q_{c9} = 0$, and Q_{c10} [W], and radiation Q_{r1}, $Q_{r2} = 0$,…, $Q_{r9} = 0$, and Q_{r10} [W] need to be estimated for the equivalent TEFC induction motor under different operating conditions.

Since the exterior of the TEFC induction motors typically consists of two different types of surface (polished surfaces of the shaft extensions and colored surfaces of the frame and end-shields), the number of the heat transfer coefficients corresponding to the radiation processes can be reduced in the following manner: $h_{r1} = h_{r10} = h_{r\mathrm{Sh}}$ – for the shaft extensions, and

$h_{r3} = h_{r4} = h_{r5} = h_{r6} = h_{r7} = h_{r8} = h_{rF}$ – for the frame and end-shields. The heat transfer coefficients h_{rSh} and h_{rF} correspond with the appropriate thermal emission coefficients $\varepsilon_{\mathrm{Sh}}$ and ε_F, respectively.

The iteration procedure for calculation of the heat transfer coefficients requires knowledge of T_s, which is initially unknown. To obtain an initial estimate of T_s, the same numerical value should be taken for all unknown heat transfer coefficients (for example 50 W/m^{2}K). Therefore, an initial estimate of T_s can be obtained from:

$$Q_{\mathrm{tot}} = \sum_{i=1}^{10} (Q_{ci,s} + Q_{ri,s}) S_i \tag{8}$$

More precisely:

$$T_s = \frac{Q_{\mathrm{tot}}}{\Sigma_c + \Sigma_r} + T_a \tag{9}$$

where

$$\Sigma_c = \sum_{i=1}^{10} h_{ci} S_i, \quad \Sigma_r = \sum_{i=1}^{10} h_{ri} S_i,$$

and Q_{tot} [W] is the total amount of power lost within the TEFC induction motor. The total power loss Q_{tot} is usually measured and consists of the following five components [17]: the stator winding losses, the iron-core losses, the rotor winding losses, the friction and windage losses and the stray losses.

The heat fluxes due to forced convection from the outer surfaces of the motor to the surrounding air are modelled in a usual manner by an equation of the form:

$$Q_{ci,s} = h_{ci}(T_s - T_a) \tag{10}$$

where $Q_{ci,s}$ and h_{ci} represent one of the aforementioned heat fluxes due to forced convection and its corresponding heat transfer coefficient.

The forced-convection heat transfer coefficients, h_{ci}, equal:

$$h_{ci} = \frac{K_{\mathrm{Nu}} \mathrm{Nu} k_t}{L_c} \tag{11}$$

where K_{Nu} is the dimensionless coefficient which equals 1 for laminar and turbulent forced convection from all the aforementioned surfaces except for turbulent forced convection from the flat and cylindrical surfaces of end-shields, Nu – the average Nusselt number which should be calculated using different empirical correlations, k_t [Wm^{-1}K^{-1}] – the thermal conductivity of the surrounding air, and L_c [m] – an appropriate characteristic length. The values of coefficient K_{Nu} for turbulent forced convection from the end-shields in this iteration procedure are specified in the following manner [9]:

$$K_{\mathrm{Nu}} = K_{\xi,y} = 1 + (1.4163 - 1)\mathrm{e}^{-4.62y} \quad - \text{ for flat outer surfaces of end-shields,} \tag{12}$$

and

$$K_{\mathrm{Nu}} = K_{\xi,y} = 1 + (1.6776 - 1)\mathrm{e}^{-13.087y} \quad - \text{ for cylindrical outer surfaces of end-shields} \tag{13}$$

where $K_{\xi,y}$ is the turbulence factor model. At a film temperature $T_f = (T_s + T_a)/2$, the thermal conductivity, k_t, the kinematic viscosity, ν [m^{2}s^{-1}], and the Prandtl number of air have been read from corresponding input data files and interpolated using a cubic spline.

The average Nusselt number correlations for 3-D shapes which are used to represent the motor exterior, together with the corresponding characteristic lengths, L_c, Reynolds numbers, and references, are presented in tab. 1. Some of these correlations are modified by introducing the Prandtl number to the appropriate power, while others are derived from existing ones for combined heat transfer by using the forced-convection correlations for a single flat plate.

The heat fluxes due to radiation from all the particular outer surfaces of the motor to the surroundings are modelled by the Stefan-Boltzmann law, that is, by the following equation:

$$Q_{ri,s} = h_{ri}(T_s - T_a) \tag{14}$$

where $Q_{ri,s}$ is one of the aforementioned heat fluxes due to radiation and h_{ri} is corresponding heat transfer coefficient, which depends on temperature in the following manner:

$$h_{ri} = \sigma_{\mathrm{SB}}\varepsilon_i(T_s^2 + T_a^2)(T_s + T_a) \tag{15}$$

where σ_{SB} is the Stefan-Boltzmann constant and ε_i is the appropriate thermal emission coefficient (ε_i equals to $\varepsilon_{\mathrm{Sh}}$, ε_F or zero).

Moreover, from iteration to iteration the coefficients h_{ci} and h_{ri} should be calculated using eqs. (11) and (15), respectively. Each new estimation for T_s should be calculated by averaging the previously estimated and newly found values of h_{ci} and h_{ri}. The iteration procedure continues until the difference between the previously estimated and the newly found T_s becomes sufficiently small. Finally, this iteration procedure uses the final value of T_s to calculate the final values of h_{ci}, h_{ri}, $Q_{ci} = Q_{ci,s}S_i$ and $Q_{ri} = Q_{ri,s}S_i$ where Q_{ci}, Q_{ri}, and S_i are one of the aforementioned heat transfer rates due to forced convection, one of the aforementioned heat transfer rates due to radiation and corresponding surface area, respectively.

When all the heat transfer rates due to forced convection and radiation are known, it is possible to determine the temperature distribution along the frame. In order to obtain the best possible longitudinal temperature profile, the following assumptions are also introduced: (1) temperatures of the drive and non-drive end-shields T_{s1} and T_{s0} are constant, unequal, T_{s1} is greater than T_{s0} and it always holds that $T_{s1} > T_s > T_{s0}$, (2) longitudinal temperature profiles $T_s(y)$ for the cooling fins and inter-fin surfaces have the same shapes and change with the distance y within the range from T_{s0} to T_{s1}, (3) maximum surface temperature along the frame T_{sM} and its corresponding longitudinal co-ordinate y_M are available based on infrared thermography or any other measurement technique, (4) temperatures of the shaft extensions are equal to the temperatures of the appropriate end-shields, and (5) all the heat transfer coefficients due to radiation are constant and depend only on the average temperature T_s.

In accordance with these assumptions for the given T_{sM} [K] and y_M [m], the following expression for the longitudinal temperature profile $T_s(y)$ [°C] is obtained:

$$T_s(y) = \frac{Q_{cj} + Q_{rj}}{[h_{cj}(y) + h_{rj}]S_j} + T_a - 273.157 \tag{16}$$

where

$$h_{cj}(y) = K_{\xi,y}h_{cj,\infty} = \frac{K_{\xi,y}}{K_{\xi,y_M}}\frac{Q_{cj} + Q_{rj}}{S_j(T_{sM} - T_a)} - h_{rj} \tag{17}$$

Table 1. Forced-convection correlations for elementary 3-D shapes

Geometry			Flow regime	Recommended correlation	L_c	Reynolds number and intended range of its application	Ref.
No.	3-D shape	Surface			[m]		
1*[a]	Rotating disk	S_1	Laminar	$\mathrm{Nu}=\frac{0.4964\,\mathrm{Re}^{1/2}}{0.6/\mathrm{Pr}+0.95/\mathrm{Pr}^{1/3}}$	r_1	$\mathrm{Re}=\frac{\Omega r_1^2}{\nu}<2.4\cdot10^5$	[18-20]
			Turbulent	$\mathrm{Nu}=0.0168\mathrm{Re}^{4/5}\mathrm{Pr}^{1/3}$	r_1	$\mathrm{Re}=\frac{\Omega r_1^2}{\nu}\geq2.4\cdot10^5$	[18-20]
3*[b]	Stationary horizontal cylinder	S_3	Laminar	$\mathrm{Nu}=0.108\mathrm{Re}^{0.656}\,\mathrm{Pr}^{1/3}$	$2r_3$	$\mathrm{Re}=\frac{2V_1r_3}{\nu}<6\cdot10^4$	[21-23]
			Turbulent			$\mathrm{Re}=\frac{2V_1r_3}{\nu}\geq6\cdot10^4$	
4*[b]	Stationary horizontal cylinder	S_4	Laminar	$\mathrm{Nu}=0.137\,\mathrm{Re}^{0.682}\,\mathrm{Pr}^{1/3}$	$2r_3$	$\mathrm{Re}=\frac{2V_1r_3}{\nu}<6\cdot10^4$	[21]
			Turbulent			$\mathrm{Re}=\frac{2V_1r_3}{\nu}\geq6\cdot10^4$	
5*[c]	Stationary horizontal finned cylinder	S_5	Laminar	$\mathrm{Nu}=\mathrm{Nu}^{(2)}\left[1-\frac{0.02H_{FE}}{D_{FE}}\right]$; $\mathrm{Nu}^{(2)}=\mathrm{Nu}^{(1)}\left[1-0.12\left(\frac{H_{FE}}{D_{FE}}\right)^{1/3}\right]$; $\mathrm{Nu}^{(1)}=0.664\,\mathrm{Re}^{1/2}\,\mathrm{Pr}^{1/3}$	L_5	$\mathrm{Re}=\frac{V_0L_5}{\nu}<6\cdot10^4$	[4, 5, 24]
			Turbulent	$\mathrm{Nu}=\mathrm{Nu}^{(2)}\left[1-\frac{0.02H_{FE}}{D_{FE}}\right]$; $\mathrm{Nu}^{(2)}=\mathrm{Nu}^{(1)}\left[1-0.09\left(\frac{H_{FE}}{D_{FE}}\right)^{1/2}\right]$; $\mathrm{Nu}^{(1)}=0.037\,\mathrm{Re}^{4/5}\,\mathrm{Pr}^{1/3}$	L_5	$\mathrm{Re}=\frac{V_0L_5}{\nu}\geq6\cdot10^4$	[4, 5, 24]
6*[c]	Stationary horizontal finned cylinder	S_6	Laminar	$\mathrm{Nu}=\mathrm{Nu}^{(1)}\left[1-0.35\left(\frac{H_{FE}}{D_{FE}}\right)^{1/3}\right]$; $\mathrm{Nu}^{(1)}=0.664\,\mathrm{Re}^{1/2}\,\mathrm{Pr}^{1/3}$	L_5	$\mathrm{Re}=\frac{V_0L_5}{\nu}<6\cdot10^4$	[4, 5, 24]
			Turbulent	$\mathrm{Nu}=\mathrm{Nu}^{(1)}\left[1-0.23\left(\frac{H_{FE}}{D_{FE}}\right)^{1/2}\right]$; $\mathrm{Nu}^{(1)}=0.037\,\mathrm{Re}^{4/5}\,\mathrm{Pr}^{1/3}$	L_5	$\mathrm{Re}=\frac{V_0L_5}{\nu}\geq6\cdot10^4$	[4, 5, 24]

→

Table 1. (continuation)

Geometry			Flow regime	Recommended correlation	L_c	Reynolds number and intended range of its application	Ref.
No.	3-D shape	Surface			[m]		
7*b	Stationary horizontal cylinder	S_7	Laminar	$\mathrm{Nu} = 0.137\,\mathrm{Re}^{0.682}\,\mathrm{Pr}^{1/3}$	$2r_3$	$\mathrm{Re} = \frac{2V_0 r_3}{\nu} < 6\cdot 10^4$	[21]
			Turbulent			$\mathrm{Re} = \frac{2V_0 r_3}{\nu} \geq 6\cdot 10^4$	
8*b	Stationary horizontal cylinder	S_8	Laminar	$\mathrm{Nu} = 1.22\,\mathrm{Re}^{0.466}\,\mathrm{Pr}^{1/3}$	$2r_3$	$\mathrm{Re} = \frac{2V_p r_3}{\nu} < 6\cdot 10^4$	[21-23]
			Turbulent			$\mathrm{Re} = \frac{2V_p r_3}{\nu} \geq 6\cdot 10^4$	
10*a	Rotating disk	S_{10}	Laminar	$\mathrm{Nu} = \frac{0.4964\,\mathrm{Re}^{1/2}}{\frac{0.6}{\mathrm{Pr}} + \frac{0.95}{\mathrm{Pr}^{1/3}}}$	r_9	$\mathrm{Re} = \frac{\Omega r_9^2}{\nu} < 2.4\cdot 10^5$	[18-20]
			Turbulent	$\mathrm{Nu} = 0.0168\,\mathrm{Re}^{4/5}\,\mathrm{Pr}^{1/3}$	r_9	$\mathrm{Re} = \frac{\Omega r_9^2}{\nu} \geq 2.4\cdot 10^5$	[18-20]

*a Correlations from [18] are corrected according to the results and correlations reported in [19, 20]. The Reynolds number is based on the angular velocity of the rotor Ω [rads^{-1}].

*b Correlations from [21] are modified by introducing the Prandtl number to the 1/3 power. This is in accordance with the forms of appropriate correlations reported in [22, 23]. It is also assumed that the transition Reynolds numbers for the surfaces S_3, S_4, S_7, and S_8 of the stationary horizontal cylinders correspond to the one for straight fins from [4, 5]. The Reynolds number is based on V_1, V_0 or V_p.

*c These correlations are derived from the correlations for combined heat transfer by forced convection and radiation from [4, 5] by using the forced-convection correlations for a single flat plate from [24]. The Reynolds number is based on V_0.

is the distance-dependent heat transfer coefficient due to forced convection from the cooling fins or inter-fin surfaces in [Wm^{-2}K^{-1}], j is the subscript denoting the cooling fins or inter-fin surfaces, $h_{cj,\infty} = \{(Q_{cj} + Q_{rj})/[S_j(T_{sM} - T_a)] - h_{rj}\}/K_{\xi,yM}$ – the heat transfer coefficient due to forced convection from the cooling fins or inter-fin surfaces that corresponds to the distance $y \to \infty$ in [Wm^{-2}K^{-1}], $K_{\xi,y}$ – the turbulence factor model for fins and inter-fin surfaces defined by [9]:

$$K_{\xi,y} = 1 + (1.8 - 1)\mathrm{e}^{-13.087y} \tag{18}$$

and K_{ξ,y_M} is the value of the turbulence factor model (18) at the distance $y = y_M$. There are only two values of the subscript j, namely 5 – for the cooling fins and 6 – for the inter-fin surfaces.

The remaining heat transfer coefficients due to forced convection from the surfaces on the drive and non-drive sides of the motor are recalculated by means of:

$$h_{ci} = \frac{Q_{ci} + Q_{ri}}{S_i(T_{s1} - T_a)} - h_{ri} \tag{19}$$

$$h_{ci} = \frac{Q_{ci} + Q_{ri}}{S_i(T_{s0} - T_a)} - h_{ri} \tag{20}$$

respectively, where the subscript i is not equal to 2, j, or 9.

Results and discussions

The proposed analytical heat transfer model is applied to the 4 and 15 kW TEFC induction motors from [25], where these motors were analyzed experimentally and by means of the lumped-parameter circuits. All the necessary input data for applying the model is also taken from [25]. Therefore, this left open the possibility to compare the results obtained by the proposed model to the existing ones.

The results related to the 4 kW motor are presented in fig. 3 and tab. 2, while the results related to the 15 kW motor are presented in fig. 4 and tab 3. Figures 3 and 4 show the longitudinal changes in the heat transfer coefficients h_{c5} and h_{c6} as well as in temperature T_s of the 4 and 15 kW motors, respectively. Each of the operating regimes in these two figures has a load torque, τ, which is approximately equal to the appropriate rated-load torque. Moreover, the supply frequencies, f, and the total power losses, Q_{tot}, are different. The distance-dependences of h_{c5} and h_{c6} are modelled by eq. (17), while the distance-dependences of T_s are modelled by eq. (16). Figures 3 and 4 also show measured data appropriate to each of the operating regimes.

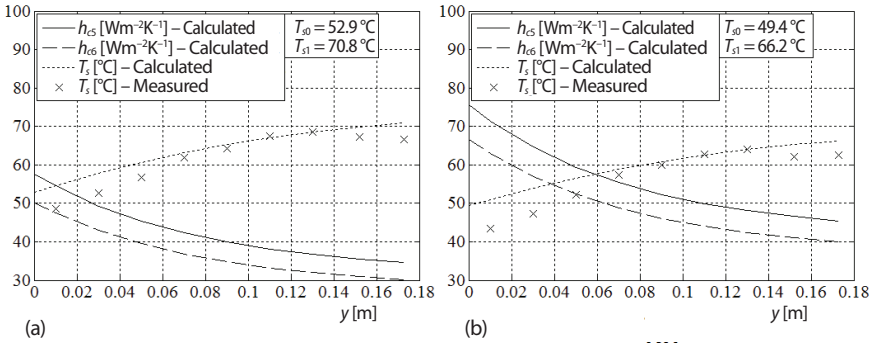

Figure 3. Longitudinal change in heat transfer coefficients and surface temperature of the 4 kW TEFC induction motor: (a) at f = 48.8 Hz, τ = 26.7 Nm, and Q_{tot} = 768 W and (b) at f = 69.9 Hz, τ = 26.6 Nm, and Q_{tot} = 861 W

Table 2. Heat transfer coefficients and heat transfer rates for the outer surfaces of the 4 kW TEFC induction motor at two different operating regimes

i	S_i	f = 48.8 Hz, τ = 26.7 Nm, and Q_{tot} = 768 W				f = 69.9 Hz, τ = 26.6 Nm, and Q_{tot} = 861 W			
		h_{ci}	Q_{ci}	h_{ri}	Q_{ri}	h_{ci}	Q_{ci}	h_{ri}	Q_{ri}
–	[m^2]	[Wm^{-2}K^{-1}]	[W]	[Wm^{-2}K^{-1}]	[W]	[Wm^{-2}K^{-1}]	[W]	[Wm^{-2}K^{-1}]	[W]
1	$6.1575\cdot10^{-4}$	15.942	0.531	5.6445	0.14514	18.355	0.557	5.4925	0.12262
2	$7.5630\cdot10^{-3}$	0	0	0	0	0	0	0	0
3	$2.9158\cdot10^{-2}$	16.187	25.799	6.7027	8.1615	20.739	29.884	6.5221	6.895
4	$2.0842\cdot10^{-2}$	25.238	28.04	6.7027	5.8339	32.666	32.863	6.5221	4.9286
5	$1.8448\cdot10^{-1}$	Fig. 3(a) – solid line	336.682	6.7027	51.638	Fig. 3(b) – solid line	399.599	6.5221	43.625
6	$8.8307\cdot10^{-2}$	Fig. 3(a) – dashed line	140.818	6.7027	24.718	Fig. 3(b) – dashed line	167.134	6.5221	20.882
7	$2.0842\cdot10^{-2}$	97.411	65.674	6.7027	5.8339	122.62	74.349	6.5221	4.9286
8	$2.9158\cdot10^{-2}$	70.447	65.969	6.7027	8.1615	80.936	68.218	6.5221	6.895
9	$6.2654\cdot10^{-3}$	0	0	0	0	0	0	0	0
10	$7.0686\cdot10^{-4}$	27.688	0.61	5.6445	0.16662	31.969	0.639	5.4925	0.14077

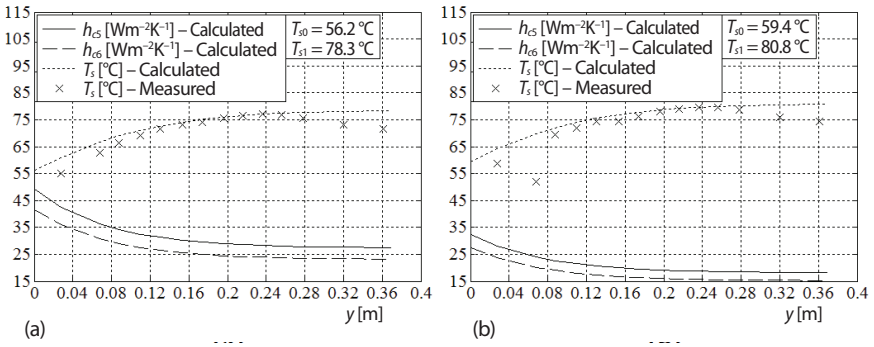

Figure 4. Longitudinal change in heat transfer coefficients and surface temperature of the 15 kW TEFC induction motor: (a) at f = 47.9 Hz, τ = 148 Nm, and Q_{tot} = 2631 W, and (b) at f = 29.7 Hz, τ = 147 Nm, and Q_{tot} = 2039 W

Table 3. Heat transfer coefficients and heat transfer rates for the outer surfaces of the 15 kW TEFC induction motor at two different operating regimes

i	S_i	f = 47.9 Hz, τ = 148 Nm, and Q_{tot} = 2631 W				f = 29.7 Hz, τ = 147 Nm, and Q_{tot} = 2039 W			
		h_{ci}	Q_{ci}	h_{ri}	Q_{ri}	h_{ci}	Q_{ci}	h_{ri}	Q_{ri}
–	[m^2]	[Wm^{-2}K^{-1}]	[W]	[Wm^{-2}K^{-1}]	[W]	[Wm^{-2}K^{-1}]	[W]	[Wm^{-2}K^{-1}]	[W]
1	$1.8096\cdot10^{-3}$	10.39	1.267	5.6421	0.42549	8.0824	1.056	5.7295	0.46428
2	$2.0029\cdot10^{-2}$	0	0	0	0	0	0	0	0
3	$6.8534\cdot10^{-2}$	12.73	58.528	6.6998	19.136	8.7454	43.948	6.8037	20.881
4	$5.1466\cdot10^{-2}$	21.635	70.683	6.6998	14.37	14.914	52.317	6.8037	15.681
5	$8.1121\cdot10^{-1}$	Fig. 4(a) – solid line	1391.432	6.6998	226.5	Fig. 4(b) – solid line	986.052	6.8037	247.16
6	$3.0496\cdot10^{-1}$	Fig. 4(a) – dashed line	446.9	6.6998	85.15	Fig. 4(b) – dashed line	316.7	6.8037	92.915
7	$5.1466\cdot10^{-2}$	84.254	154.992	6.6998	14.37	58.631	116.866	6.8037	15.681
8	$6.8534\cdot10^{-2}$	52.637	127.997	6.6998	19.136	41.21	108.633	6.8037	20.881
9	$1.0653\cdot10^{-2}$	0	0	0	0	0	0	0	0
10	$1.9635\cdot10^{-3}$	20.203	1.374	5.6421	0.46168	15.619	1.146	5.7295	0.50378

Generally, the length of the frame can be divided into three zones: drive end-winding, stator core, and non-drive end-winding. The lengths of the drive and non-drive end-winding zones are approximately equal to each other and these lengths amount to 0.035 and 0.07 m for the 4 and 15 kW motors, respectively. The lengths of the stator core zones of the 4 and 15 kW motors are 0.105 and 0.23 m, respectively. Accordingly, the results shown in figs. 3 and 4 indicate that a good agreement exists between the calculated and measured data for the stator core zones of both motors. The percent deviations between the measured data and the data obtained by the proposed analytical model for stator core zones are lower than 12.5% for the 4 kW motor and lower than 6.3% for the 15 kW motor. Similarly, for end-winding zones, the percent deviations are between 3.7~17.2% for the 4 kW motor and between 6 ~ 10.9% for the 15 kW motor. Based on the results shown in these figures, it can also be seen that the percent deviation gradually increases as the supply frequency (that is, the angular velocity of the rotor) increases.

Tables 2 and 3 summarize the analytical results obtained for all the operating regimes of the 4 and 15 kW motors. For each operating regime a set of 15 to 17 iterations was needed. The heat transfer coefficients and the heat transfer rates are calculated using a MATLAB

program. From the simulation results it can be noticed that the average temperature, T_s, equals to 61.76, 56.257, 61.675, and 64.781 °C for the operating regime presented in figs. 3(a), 3(b), 4(a), and 4(b) (at the air temperature T_a = 20 °C), respectively. From the same simulations it can be noticed that the average values of the coefficients h_{c5} and h_{c6} equal to: 43.701 and 38.186 W/m^{2}K – for the regime presented in fig. 3(a), 59.741 and 52.201 W/m^{2}K – for the regime presented in fig. 3(b), 41.158 and 35.163 W/m^{2}K – for the regime presented in fig. 4(a), 27.144 and 23.19 W/m^{2}K – for the regime presented in fig. 4(b), respectively. Moreover, the temperature T_{sM} and its corresponding coordinate y_M are taken from measured data, figs. 3(a), 3(b), 4(a) and 4(b).

In comparison with the result calculated by the lumped-parameter circuit from [25], the average temperature T_s = 61.675 °C of the 15 kW motor at rated load conditions is lower by 8.125 °C. However, that is not the case with the 4 kW motor at rated load conditions. For the 4 kW motor at rated load conditions this difference is only 0.16 °C. Further comparison of differences between these two models would be unnecessary.

By knowing the amounts of heat dissipated through the end-shields, it is possible to calculate all the heat transfer coefficients of the motor exterior with a satisfactory accuracy [25]. According to [25], the amounts of heat dissipated through the drive and non-drive end-shields, respectively, are 9, and 19% of Q_{tot} for the 4 kW motor at rated operation, and 6, and 12% of Q_{tot} for the 15 kW motor at rated operation. According to tabs. 2 and 3, the portions of heat dissipated through the drive and non-drive end-shields amount to: (1) 8.833% and 18.963% – for the regime presented in fig. 3(a), (2) 8.661% and 17.932% – for the regime presented in fig. 3(b), (3) 6.185% and 12.029% – for the regime presented in fig. 4(a), and (4) 6.514% and 12.852% – for the regime presented in fig. 4(b). The portions (1) and (3) agree well with the corresponding data given in [25]. Moreover, it can be noticed that the portions of heat dissipated through the end-shields decrease as the supply frequency increases (or increase as f decreases).

Conclusions

The conclusions arising from the present paper are as follows.

- The proposed approach to analytical modelling of steady-state heat transfer from the exterior of TEFC induction motors excludes rough approximations, it is scientifically and empirically based, rather simple and provides more accurate results in comparison with the common ones, which are based on the lumped-parameter circuits.
- The procedure for modelling the geometry of TEFC induction motors is based on empirically confirmed facts and its implementation does not require a large amount of input data.
- A set of correlations, based on the one-nth-power law, for the profiles of air-flow velocity along the cooling channels was taken from [9] and successfully applied to the proposed analytical model.
- Three models for the turbulence factor were taken from [9] and successfully introduced to the proposed analytical model. The turbulence factor models apply to all types of TEFC induction motors.
- A set of modified and corrected correlations for heat transfer due to forced convection from the rotating disks, stationary horizontal cylinders, fins and inter-fin surfaces is proposed and successfully applied.
- According to figs. 3 and 4, the percent deviations between the measured surface temperatures and the surface temperatures obtained by the proposed analytical model are between 0~17.2% for the 4 kW motor at given operating regimes and between 0~10.9% for the 15 kW motor at given operating regimes. The deviation increases as the supply frequency increases.

- The presented analytical results correspond to a greater or lesser extent to the results obtained by the lumped-parameter circuits. For the 4 and 15 kW motors at rated load conditions the surface temperatures differ amongst themselves by 0.16 and 8.125 °C, respectively.
- The portions of heat dissipated through the drive and non-drive end-shields decrease as the supply frequency increases.
- The heat transfer coefficients obtained by means of the proposed analytical model can be used further for the analytical thermal modelling of the interior parts of the induction motors or for the appropriate finite element analysis.

Acknowledgment

This research was conducted within the project 259873 funded by the Academy of Finland.

References

[1] Staton, D. A., Cavagnino, A., Convection Heat Transfer and Flow Calculations Suitable for Electric Machines Thermal Models, *IEEE Transactions on Industrial Electronics, 55* (2008), 10, pp. 3509-3516
[2] Romo, J. L., Adrian, M. B., Prediction of Internal Temperature in Three-Phase Induction Motors with Electronic Speed Control, *Electric Power Systems Research, 45* (1998), 2, pp. 91-99
[3] Huai, Y., *et al*., Computational Analysis of Temperature Rise Phenomena in Electric Induction Motors, *Applied Thermal Engineering, 23* (2003), 7, pp. 779-795
[4] Ghai, M. L., Jakob, M., Local Coefficients of Heat Transfer for Straight Fins, *American Society of Mechanical Engineers, Paper No. 50-S-18,* 1950
[5] Ghai, M. L., Heat Transfer in Straight Ffins, in: *General Discussion on Heat Transfer*, American Society of Mechanical Engineers, New York, USA, 1951, pp. 180-182
[6] Valenzuela, M. A., Tapia, J. A., Heat Transfer and Thermal Design of Finned Frames for TEFC Variable Speed Motors, *Proceedings,* 32nd Annual Conference on IEEE Industrial Electronics – IECON 2006, Paris, 2006, pp. 4835-4840
[7] Valenzuela, M. A., Tapia, J. A., Heat Transfer and Thermal Design of Finned Frames for TEFC Variable-Speed Motors, *IEEE Transactions on Industrial Electronics, 55* (2008), 10, pp. 3500-3508
[8] Fuchs, E. F., Masoum, M. A. S., *Power Quality in Power Systems and Electrical Machines*, 2nd ed., Elsevier Academic Press, New York, USA, 2008
[9] Klimenta, D. O., Hannukainen, A., An Approximate Estimation of Velocity Profiles and Turbulence Factor Models for Air-Flows along the Exterior of TEFC Induction Motors, *Thermal Science*, in this issue pp. 1515-1527
[10] Xypteras, J., Hatziathanassiou, V., Thermal Analysis of an Electrical Machine Taking into Account the Iron Losses and the Deep-Bar Effect, *IEEE Transactions on Energy Conversion, 14* (1999), 4, pp. 996-1003
[11] Chen, Y.-C., *et al*., CFD Thermal Analysis and Optimization of Motor Cooling Fin Design, *Proceedings,* ASME Summer Heat Transfer Conference – HT2005, San Francisco, Cal., USA, 2005, ID HT2005-72567, pp. 1-5
[12] Hewitt, G. F., Hall-Taylor, N. S., *Annular Two-Phase Flow*, Pergamon Press, Oxford, UK, 1970
[13] Balachandran, P., *Engineering Fluid Mechanics*, PHI Learning Private Limited, New Delhi, 2011, pp. 232-275
[14] Webster, J. G., Eren, H., *Measurement, Instrumentation, and Sensors Handbook: Spatial, Mechanical, Thermal, and Radiation Measurement*, 2nd ed., CRC Press, Taylor & Francis Group, LLC, Boca Raton, Fla., USA, 2014, pp. 57.6-57.8
[15] Holland, F. A., Bragg, R., *Fluid Flow for Chemical Engineers*, 2nd ed., Butterworth-Heinemann, Oxford, UK, 1995, pp. 85-88
[16] Kovalev, E. B., *et al*., Heat Release in Channels between Frame-Ribbing of Enclosed Asynchronous Motors, *Elektrotekhnika, 36* (1965), 11, pp. 27-29
[17] Chapman, S. J., *Electric Machinery Fundamentals*, 5th International edition, McGraw-Hill, Inc., N. Y., 2011, pp. 307-403
[18] Mills, A. F., *Heat Transfer*, Richard D. Irwin, Inc., Homewood, Ill., USA, 1992, pp. 330-333

[19] Cobb, E. C., Saunders, O. A., Heat Transfer From a Rotating Disk, *Proceedings of the Royal Society of London, Series A , Mathematical and Physical Sciences, 236* (1956), 1206, pp. 343-351
[20] Axcell, B. P., Thianpong, C., Convection to Rotating Disks with Rough Surfaces in the Presence of an Axial Flow, *Experimental Thermal and Fluid Science, 25* (2001), 1-2, pp. 3-11
[21] Wiberg, R., Lior, N., Heat Transfer from a Cylinder in Axial Turbulent Flows, *International Journal of Heat and Mass Transfer, 48* (2005), 8, pp. 1505-1517
[22] Kobus, C. J., Shumway, G., An Experimental Investigation into Impinging Forced Convection Heat Transfer from Stationary Isothermal Circular Disks, *International Journal of Heat and Mass Transfer, 49* (2006), 1-2, pp. 411-414
[23] Kobus, C. J., Wedekind, G. L., An Experimental Investigation into Forced, Natural and Combined Forced and Natural Convective Heat Transfer from Stationary Isothermal Circular Disks, *International Journal of Heat and Mass Transfer, 38* (1995), 18, pp. 3329-3339
[24] ***, ASHRAE, Chapter 4 – Heat Transfer, in: *2009 ASHRAE Handbook – Fundamentals*, American Society of Heating, Refrigerating and Air-Conditioning Engineers, Inc., Atlanta, Geo., USA, 2009, pp. 4.1-4.34
[25] Kylander, G., Thermal Modelling of Small Cage Induction Motors, Ph. D. thesis, School of Electrical and Computer Engineering, Chalmers University of Technology, Gothenburg, Sweden, 1995

Paper submitted: June 26, 2015
Paper revised: April 22, 2016
Paper accepted: April 22, 2016